Ab Initio Gga+U and Experimental Study of the Wurtzite Structure of ZnO for Dye-Sensitized Solar Cells Application

Irungu M. Kahura[1*]; Sharon Kiprotich[1]; Jatani Ungula[2]

[1]Department of Physical and Biological Sciences, Murang'a University of Technology P.O Box 75-10200 Murang'a, Kenya

[2]Department of Physics, Kenya Methodist University, P.O Box 267 – 60200, Meru, Kenya

[*]Corresponding Author

DOI: https://doi.org/10.51584/IJRIAS.2025.10120026

Received: 21 December 2025; Accepted: 27 December 2025; Published: 05 January 2026

ABSTRACT

Zinc oxide (ZnO) is an extensively utilized, versatile compound implemented in a diverse scope of technological applications. In dye-sensitized solar cells (DSSCs), the attainable nanostructures, inherent transparency and tunable electronic properties of ZnO can be integrated to confer high level device properties. ZnO is a complex compound with substantial and intricate defect chemistry and its properties are exceptionally sensitive to the functional utilized in the computing and experimental processes. Consequently, engineering of the band edges in Wurtzite ZnO (W-ZnO) for DSSCs application has not yet been exhausted. The W-ZnO was synthesized using sol-gel method while the computations were performed using density functional theory (DFT) as implemented in the Quantum ESPRESSO code. The generalized gradient approximation with Perdew-Burke-Ernzerhof was utilized as the exchange correlation functional. Investigations of the structural, electronic and optical properties of W-ZnO were carried out using both computational and experimental techniques. In the experimental analysis, the influence of growth temperature on ZnO was investigated, whereas in the computational study, the impact of varying the Hubbard U parameter on pure ZnO was examined. The structural properties of the materials have been found to be consistent with previous observations in literature with a slight decrease in lattice parameters in the DFT+U calculations. W-ZnO was observed to display a direct band gap at gamma. The energy band gaps of, 0.79 eV, 1.45 eV, 3.19 and 3.33 eV in the standard DFT, DFT + U_d, DFT+U_d +Up calculations and experimental values were obtained respectively. Generally, W-ZnO was found to have low absorption ability and high transmittance in the visible spectrum which were in close correlation with the experimental values obtained which therefore make them suitable candidates for DSSCs application.

Keywords: DFT+U; DSSCs; Solgel; Wurtzite ZnO; Structural properties.

INTRODUCTION

Zinc oxide (ZnO) is a widely studied II–VI semiconductor due to its wide band gap (3.37 eV), large exciton binding energy (60 meV), high electron mobility, and rich defect chemistry, making it suitable for numerous optoelectronic applications such as light-emitting diodes, UV lasers, and particularly dye-sensitized solar cells (DSSCs) [1,2]. Its inherent ability to be synthesized in various nanostructures including nanorods, nanowires, and nanoparticles adds to its versatility in solar cell architectures [3]. Compared to the extensively studied TiO_2, ZnO offers higher electron mobility and comparable conduction band energy levels, providing potential for improved charge transport and reduced recombination in DSSCs [4]. The wurtzite (W-ZnO) crystal structure is the most thermodynamically stable phase of ZnO under ambient conditions. It exhibits anisotropic properties that can be tuned through morphology, doping, and structural engineering [5]. However, the performance of ZnO-based photoanodes in DSSCs has been constrained by inherent defects such as oxygen vacancies and zinc interstitials, which affect optical absorption, charge carrier recombination, and overall efficiency [6]. To better understand and control these properties, computational methods such as Density Functional Theory (DFT) are widely used. Standard DFT calculations typically underestimate the band gap of ZnO, a limitation that can be addressed using correction methods like DFT+U, which applies on-site Coulomb

interactions to localized orbitals [7]. The choice of exchange-correlation functional, such as the Perdew–Burke–Ernzerhof (PBE) formulation under the Generalized Gradient Approximation (GGA), significantly influences the accuracy of predicted material properties [8]. Recent studies have shown that integrating computational techniques with experimental synthesis, such as the sol-gel method, enables a comprehensive understanding of ZnO's electronic and optical behavior [9]. This dual approach allows validation of theoretical predictions with real-world measurements. In particular, W-ZnO has shown promising characteristics such as direct band gaps at the Γ-point and high transmittance in the visible region, confirming its potential as a photoanode material in DSSCs [10].

METHODOLOGY

Experimental Procedures

The synthesis of samples for this study followed the same procedure as that of Chapter 4. ZnO nanostructures were prepared from aqueous solutions of zinc acetate dehydrate [Zn $(CH_3COO)_2$. $2H_20$] and sodium hydroxide (NaOH). In the three-neck glass flask, zinc acetate dehydrate was dissolved in ethanol to a concentration of 0.015 M and the resulting solution was heated, under constant stirring, to different growth temperatures (RT, 35, 45, 55, 65 and 75 °C). After achieving a desired temperature of growth, a solution of NaOH was added slowly (dripped for 60 minutes) into the three-neck glass flask containing the [Zn $(CH_3COO)_2$. $2H_20$] aqueous solution under continual stirring. In this procedure the desired reaction temperature was constantly maintained. The suspension formed with the dropping of 0.06 M alkaline aqueous solution to zinc acetate dehydrate solution was kept stirred for two hours at the same growth temperature and allowed to stand for some time till gel like solution was formed. The material was then filtered and washed several times with deionized water. The washed sample was dried at 60 °C in oven for one hour and one portion of it annealed at 600 °C for 1 hour. The yield of the ZnO nanostructures by this method is about 95%. The particle size and morphology and the structural and luminescent properties of the as-synthesized particles were examined by means of scanning electron microscopy, X-ray diffraction, UV-Vis spectroscopy and photoluminescence spectroscopy.

Computational Procedures

Ab initio calculations were conducted utilizing the density functional theory (DFT) framework as implemented in the Quantum ESPRESSO (QE) software [11]. Self-consistent calculations were executed to address the Kohn-Sham equations within the Generalized Gradient Approximation, employing the Perdew-Burke-Ernzerhof (GGA-PBE) exchange-correlation functional [12]. The unit cell of W-ZnO comprises four atoms, specifically two zinc (Zn) atoms and two oxygen (O) atoms. To ensure the precision of the results, structural optimization was performed. The convergence of k-points was assessed, ranging from 3 × 3 × 1 to 18 × 18 × 16, with increments of 2 × 2 × 2. Additionally, the kinetic energy cut-off (Ecut) was optimized within a range of 10 to 100 Ry, with steps of 5 Ry. Following this, lattice constant optimization was conducted utilizing the converged k-point and cut-off energy values, achieving convergence with a criterion set at 10^{-4} Ry. The K-point sampling of the Brillouin zone was implemented using the Monkhorst and Pack method, establishing a grid of 8 × 8 × 6 K-points. Electronic band structure calculations were performed employing both the GGA and GGA+U methodologies. This comparative analysis was necessary due to the tendency of Local Density Approximation (LDA) and GGA functionals to underestimate the electronic band gaps of materials. The THERMO-PW software was utilized to compute both the real and imaginary components of the dielectric function under standard DFT and DFT+U frameworks.

RESULTS AND DISCUSSION

Structural Properties

The structural parameters of wurtzite ZnO obtained using GGA, GGA+U_d, and GGA+U_d+U_p are summarized in Table 1 and compared with available experimental data. As expected, the conventional GGA approach overestimates the lattice constants a=3.289 Å and c=5.289 Å relative to the experimental values of 3.259 Å and 5.234 Å, respectively. This overestimation leads to a larger equilibrium volume (V_0=49.39 Å^3) and slightly elongated Zn–O bond length (1.9993 Å), which is a well-known limitation of standard GGA due to the underestimation of electron–electron interactions in localized states [13]. Upon introducing the Hubbard U

correction on the Zn-3d orbitals (GGA+U_d), both lattice constants decrease to 3.276 Å and 5.251 Å, accompanied by a reduction in equilibrium volume to 49.26 Å³. This contraction reflects improved localization of the Zn-3d electrons and a more realistic description of Zn–O bonding. Consequently, the Zn–O bond length shortens slightly to 1.9982 Å, while the c/a ratio (1.603) moves closer to the experimental value (1.601), indicating enhanced structural accuracy.

Table 1: Structural parameters of W-ZnO from GGA+U and experiment

Method	a (Å)	c(Å)	c/a	V_0 (Å³)	Bond Length (Å)	Bond Angle (°)
GGA	3.289	5.289	1.608	49.39	1.9993	108.37
GGA + Ud	3.276	5.251	1.603	49.26	1.9982	108.41
GGA + Ud + Up	3.269	5.211	1.594	48.84	1.9975	108.45
Experimental	3.259	5.234	1.601	48.143	1.9844	108.1

Further inclusion of the U correction on O-2p orbitals (GGA+U_d+U_p) results in the smallest lattice parameters (a=3.269 Å and c=5.211 Å) and equilibrium volume (V0=48.84 Å³) among the three methods, showing the closest overall agreement with experimental data. The Zn–O bond length (1.9975 Å) approaches the experimental value of 1.9844 Å, suggesting stronger Zn–O interactions due to improved treatment of O-2p states [14]. Additionally, the gradual increase in the O–Zn–O bond angle from 108.37° (GGA) to 108.45° (GGA+U_d +U_p) indicates a subtle but systematic adjustment of the tetrahedral geometry toward the ideal wurtzite structure. Overall, the results demonstrate that the combined GGA+Ud_dd+U_p approach provides the most reliable structural description of W-ZnO, effectively correcting the GGA overestimation and yielding lattice parameters, bond lengths, and volumes in excellent agreement with experimental observations.

The X-ray diffraction (XRD) patterns of ZnO nanoparticles synthesized at different growth temperatures are presented in Figure 1. All diffraction peaks can be indexed to the hexagonal wurtzite structure of ZnO, indicating phase purity and the absence of secondary phases within the detection limit of the XRD technique. As the growth temperature increases from 35 to 75 °C, a clear enhancement in crystallinity is observed. Specifically, the average crystallite size increases from 27.6 to 34.2 nm, suggesting that higher growth temperatures promote grain growth through enhanced atomic diffusion and reduced nucleation density. In addition, the XRD peak broadening systematically decreases with increasing growth temperature, while the peak intensities become sharper and more pronounced. This behavior confirms an improvement in crystal quality and a reduction in lattice strain and structural defects at elevated growth temperatures, in agreement with earlier reports [15]. The observed sharpening of diffraction peaks reflects improved ordering within the ZnO lattice and enhanced coherence length of diffracting domains.

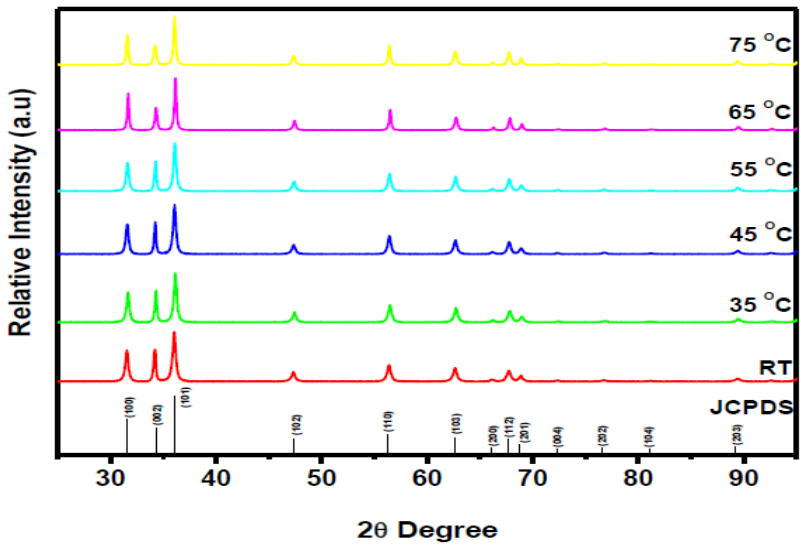

Figure 1: X- ray powder diffraction pattern for ZnO nanoparticles prepared at different growth temperature.

ISSN No. 2454-6194 | DOI: 10.51584/IJRIAS |Volume X Issue XII December 2025

A continuous increase in Zn–O bond length with increasing growth temperature is also observed. The average calculated bond length of 1.9873 Å is slightly larger than the reported Zn–O bond length of 1.9767 Å for ZnO unit cells and neighboring atoms [16]. This minor expansion can be attributed to thermal effects and lattice relaxation occurring during crystal growth at higher temperatures. Nevertheless, the calculated bond lengths show good agreement with the standard Zn–O bond length values, as summarized in Table 2, confirming the structural integrity of the ZnO lattice. Furthermore, the c/a ratio is found to decrease with increasing internal parameter uuu, indicating subtle distortions in the wurtzite lattice. This variation occurs in such a way that the four Zn–O tetrahedral bond distances remain nearly constant, accompanied by a redistribution of the tetrahedral bond angles rather than significant bond stretching [16]. The average c/a ratio of approximately 1.603 is slightly lower than the ideal value for pure ZnO (1.604), suggesting a minor deviation from the ideal wurtzite geometry due to temperature-induced lattice adjustments. The interplanar spacing is also observed to increase with growth temperature, as evidenced by a slight shift of diffraction peaks toward lower 2θ values. This shift indicates lattice expansion and increased d-spacing, which can be attributed to thermal effects and reduced residual stress within the crystal lattice at higher growth temperatures [17]. Overall, the XRD analysis confirms that increasing growth temperature enhances the crystallinity, structural ordering, and lattice stability of ZnO nanoparticles.

Table 2: Experimental structural properties of ZnO nanoparticles.

Temperature ($°C$)	Crystallite size (nm)	Lattice Constants			Positional parameter, u	Zn-O Bond length, L
		a (Å)	c (Å)	Ratio, c/a		
35	27.6	3.2595	5.2283	1.60402	0.37955	1.9844
45	28.4	3.2655	5.2379	1.60401	0.37956	1.9880
55	29.8	3.2663	5.2319	1.60178	0.37992	1.9879
75	34.2	3.2686	5.2343	1.60138	0.37998	1.9889

Electronic Properties

The electronic band structure of ZnO was first evaluated using plain DFT, as shown in Figure 2a. The calculated band gap of 0.79 eV is significantly underestimated compared to the experimentally reported value of 3.37 eV. This pronounced discrepancy is a well-known limitation of conventional DFT approaches based on the LDA) and GGA. These methods suffer from self-interaction errors and an incomplete treatment of exchange–correlation effects, particularly in systems containing localized d and p electrons [14]. In the case of ZnO, the strong hybridization between Zn-3d and O-2p orbitals is inadequately described, leading to an artificial upward shift of the valence band maximum and a narrowing of the energy separation between the valence and conduction bands [18, 19]. To mitigate this shortcoming, the on-site Coulomb interaction, commonly referred to as the Hubbard U correction, was introduced to better account for the localized nature of the Zn-3d electrons. Upon applying Ud to the Zn-3d orbitals (DFT+U_d), the calculated band gap increases to 1.45 eV, as illustrated in Figure 2b. This improvement reflects enhanced localization of the Zn-3d states, which reduces their spurious hybridization with the O-2p orbitals and shifts the valence band toward lower energies [20]. Although the resulting band gap remains smaller than the experimental value, the noticeable increase confirms that the Hubbard correction partially resolves the electron correlation problem inherent in plain DFT.

ISSN No. 2454-6194 | DOI: 10.51584/IJRIAS |Volume X Issue XII December 2025

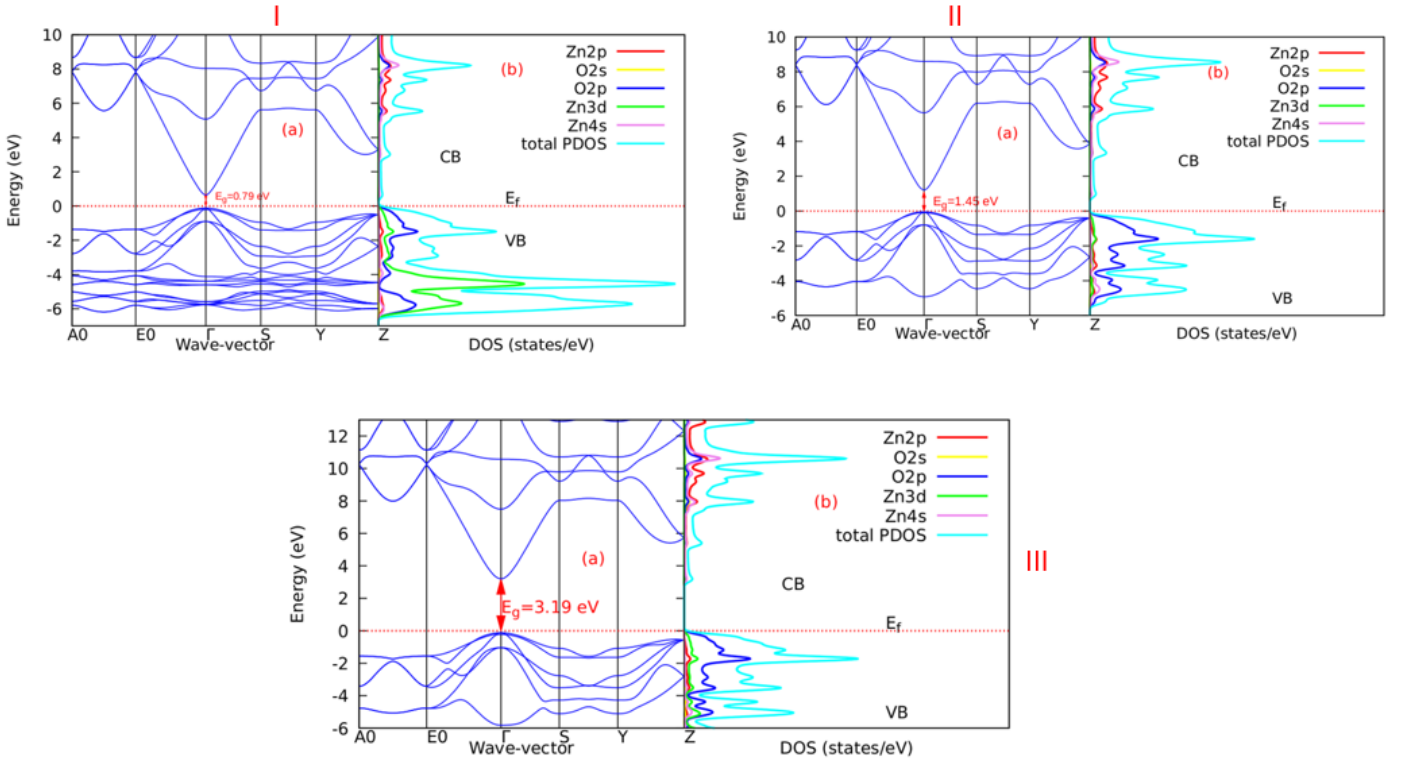

Figure 2: Band structure and density of state of W-ZnO using (I) Standard DFT, (II) DFT+$U_{d(10eV)}$ and (III) DFT + $U_{d(10eV)}$ + $U_{p(8eV)}$ approximation

A further and more substantial correction is achieved by extending the Hubbard U treatment to the O-2p orbitals in addition to the Zn-3d states (DFT+U_d+U_p). As shown in Figure 2c, this combined correction leads to a significant widening of the band gap to 3.19 eV, which is in close agreement with the experimental band gap of ZnO. The inclusion of Up effectively lowers the O-2p–derived valence band maximum, thereby restoring a more realistic separation between the valence and conduction bands [21]. This result highlights the critical role of both Zn-3d and O-2p orbitals in determining the electronic structure of ZnO and demonstrates that a balanced treatment of electron correlation in both sub-systems is necessary for accurate band-gap prediction.

Overall, the progressive increase in the band gap from plain DFT to DFT+U_d and finally to DFT+U_d+U_p clearly demonstrates the effectiveness of the Hubbard U approach in correcting the intrinsic limitations of standard DFT methods. The excellent agreement achieved with the experimental band gap validates the reliability of the DFT+U_d+U_p framework for describing the electronic properties of ZnO. Consequently, this approach provides a robust theoretical basis for predicting and optimizing the optoelectronic performance of ZnO-based materials in applications such as dye-sensitized solar cells and other photovoltaic and photonic devices [21, 22].

Optical Properties

Understanding the optical response of semiconductor materials is essential for evaluating their suitability in optoelectronic and photovoltaic applications, as these properties govern light absorption, reflection, and propagation within the material [23]. Figure 3(a) presents the UV–Vis diffuse reflectance spectra of ZnO measured at room temperature (RT) and at elevated temperatures (35–75 °C). All samples exhibit a sharp absorption edge in the near-UV region around ~380–400 nm, which is characteristic of the intrinsic band-to-band electronic transitions in wurtzite ZnO [24]. The high reflectance in the visible region (>400 nm), reaching approximately 85–90%, indicates good optical transparency and low absorption of visible light, which is desirable for optoelectronic and photoanode applications [25]. A slight increase in reflectance intensity and a marginal shift of the absorption edge toward longer wavelengths with increasing temperature are observed, suggesting subtle temperature-induced modifications in the electronic structure, likely associated with lattice expansion and enhanced electron–phonon interactions.

ISSN No. 2454-6194 | DOI: 10.51584/IJRIAS |Volume X Issue XII December 2025

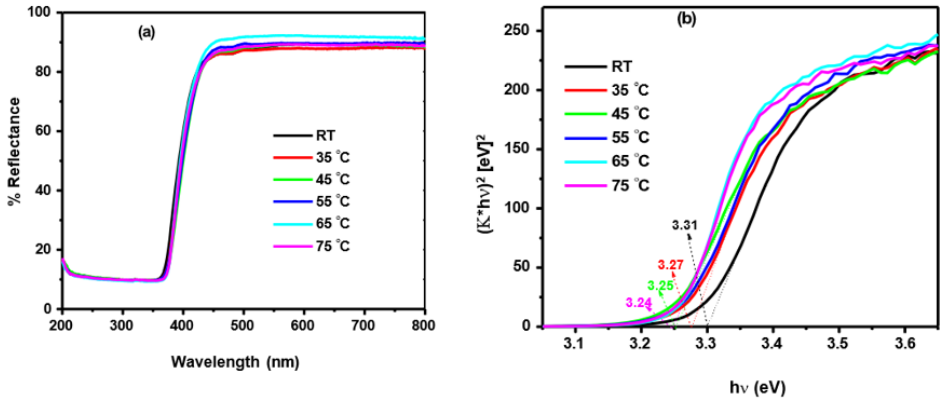

Figure 3: The (a) reflectance and (b) absorption spectra of ZnO nanoparticles prepared at various temperature.

Figure 3(b) shows the corresponding Tauc plots, absorption versus photon energy, used to estimate the direct optical band gap of ZnO at different temperatures. The linear extrapolation of the absorption edge yields band gap values that decrease systematically with increasing temperature. The band gap energy of ZnO was estimated using Kubelka-Munk remission function [21], or direct transitions. The estimated band gap reduced from 3.31 to 3.24 eV with the increase in the growth temperature as shown in Figure 3(b). Sharma et al [22] reported that the band gap for ZnO decreased due to tensile strain while compressive strain results into an increase of the band gap. A compressed lattice is expected to provide a wide band gap because of the increased repulsion between oxygen 2p and Zinc 4s bands. The estimated band gap is; however, lower than that of the bulk ZnO (3.37ev) [26, 27]. This band gap reduction may be due to surface defects density of undoped ZnO [28].

Figure 4 presents the percentage transmittance of ZnO thin films recorded at four characteristic wavenumbers (885, 1413, 1505, and 3394 cm^{-1}) as a function of growth temperature from room temperature (RT) to 75 °C. At RT, all films demonstrate very high optical transparency, with transmittance values exceeding 96% across all wavenumbers. The highest transmittance is observed at 885 cm^{-1}, indicating minimal absorption losses and good optical quality of the ZnO films deposited at ambient conditions [29]. As the growth temperature increases to 35 °C and 45 °C, a noticeable reduction in transmittance occurs for all measured wavenumbers. This decline is most pronounced at 1413 cm^{-1}, suggesting enhanced absorption or scattering effects, possibly arising from temperature-induced structural modifications, increased defect density, or changes in vibrational modes associated with Zn–O bonding [30]. Upon further temperature increase to 55 °C and 65 °C, the transmittance trends become less uniform, reflecting a complex interplay between film densification, grain growth, and defect formation. In particular, at 65 °C, the sharp decrease to approximately 91.7% at 1413 cm^{-1} indicates stronger interaction between the incident radiation and thermally activated vibrational states.

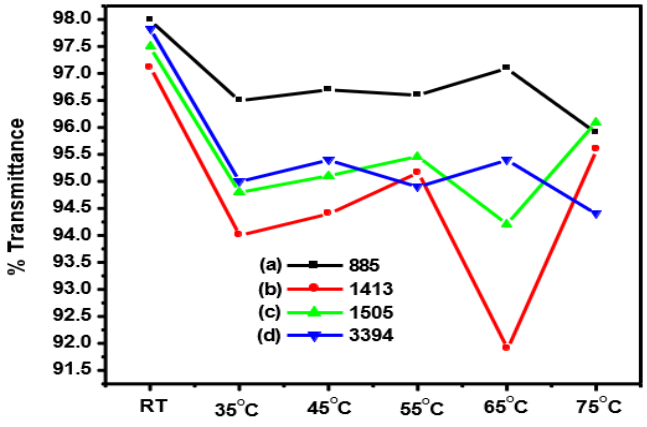

Figure 4: Transmittance (%) of ZnO at different growth temperature

At the highest growth temperature of 75 °C, an improvement in transmittance is observed for most wavenumbers, implying partial recovery of optical transparency. This enhancement may be attributed to improved crystallinity and reduced scattering centers due to better atomic rearrangement at elevated

temperatures [31]. Overall, the results demonstrate that the optical transmittance of ZnO thin films is strongly dependent on both growth temperature and wavenumber, with superior transparency achieved at lower temperatures and selectively at specific vibrational modes. First-principles calculations based on DFT were employed to provide valuable insights into the dielectric behavior and related optical constants as a function of photon energy. In this context, the optical properties of the material were systematically analyzed to establish the influence of different exchange–correlation corrections on its dielectric and refractive characteristics. The graphs depicted in Figure 5(a–f) display the relationship between optical properties and energy in eV computed in DFT technique. In reference to Figure 5(a), the electronic portion of the static dielectric function, is 8.52, 6.02 and 5.16 for DFT, DFT + U_d and DFT+U_d +U_p calculations respectively. The calculation of refractive indices is achieved by taking the square roots of the specified values [32], which are summarized in Table 3.

Table 3: Real dielectric function at 0 eV$\{\varepsilon_1(0)\}$, refractive index (n), absorption critical points and reflectivity at 0 eV (R_0)

	$\varepsilon_1(0)$	Refractive index	Absorption critical points	R(0)
DFT	8.52	2.92	0.78	0.24
DFT + U_d	6.02	2.45	1.44	0.15
DFT+U_d +U_p	5.16	2.27	3.19	0.09

From the table, introducing the Hubbard U term leads to a decrease in both the static dielectric constant $\varepsilon_1(0)$ and the refractive index. In the energy range of 5.1–5.8 eV, the negative curve indicates complete attenuation of radiation, where ZnO exhibits metallic behavior [32]. The imaginary dielectric function $\varepsilon_2(\omega)$, shown in Figure 5(b), links optical and electronic properties, with critical onset energies at 0.78, 1.46, and 3.19 eV for DFT, DFT+Ud, and DFT+Ud+Up, respectively—values that align with the computed band gaps. The $\varepsilon(\omega)$ spectrum shows three main peaks at 5.12, 10.4, and 13.6 eV, representing transitions between O-2p to Zn-4s, O-2p to Zn-3d, and O-2s to Zn-3d states [33]. The absorption coefficient, which indicates how light diminishes through a medium, is frequency-dependent and reflects interband transitions. Figure 5(c) shows absorption edges at 0.78, 1.44, and 3.19 eV for DFT, DFT+U_d, and DFT+U_d+U_p respectively. Unlike standard DFT, which predicts absorption even in the infrared, the DFT+U_d+U_p approach suggests ZnO remains transparent to much of the solar spectrum, allowing more light to reach the dye for photoemission [34–38]. The refractive index, which measures light bending, is shown in Figure 5(d) and listed in Table 3. Although it decreases across the DFT methods, it remains sufficiently high (above 1.8) for DSSC applications [35-39]. A sharp drop in the refractive index dispersion curve beyond the initial peak indicates that at higher photon energies, ZnO loses transparency and starts absorbing radiation.

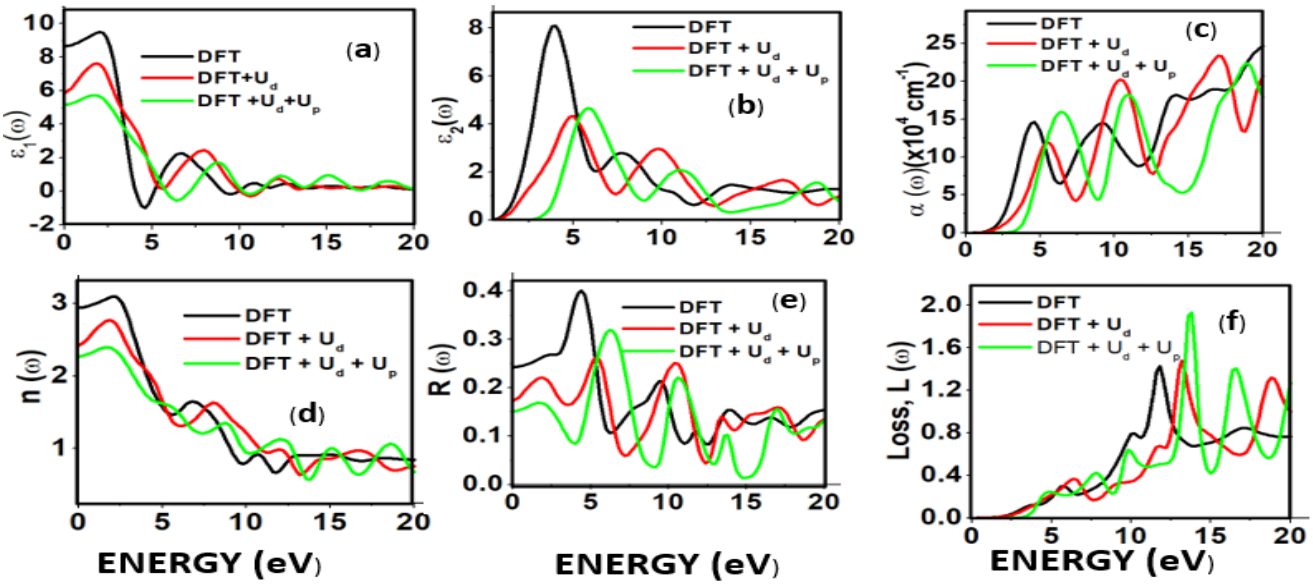

Figure 5: The (a) real (b) imaginary part of the dielectric constant, (c) absorption coefficient, (d)refractive index, (e) reflectivity and (f) energy loss as a function of the energy in eV of ZnO using DFT, DFT + U_d and DFT+U_d +U_p

Reflectivity provides insights into the surface interaction of a material with incident light [35]. As illustrated in Figure 5(e), the reflectivity at zero photon energy (R_0) is notably low. According to Table 4, the DFT+U_d+U_p method predicts the lowest reflectivity for W-ZnO, suggesting that the material reflects minimal solar radiation, thereby allowing more light to penetrate and reach the dye in DSSC applications [39]. The reflectivity spectra show prominent peaks around 4.9 eV, 5.1 eV, and 5.8 eV for DFT, DFT+U_d, and DFT+U_d+U_p methods, respectively, followed by a sharp decline in reflectivity beyond these energies. Energy loss, denoted as L (ω), quantifies how much energy a fast-moving electron loses as it travels through a material. Figure 5(f) shows negligible energy loss up to 4.0 eV across all computational approaches. Beyond this energy, the loss function increases gradually, reaching maximum values at approximately 12.8 eV for DFT, 14.2 eV for DFT+Ud, and 15.4 eV for DFT+U_d+U_p. This trend indicates that W-ZnO retains most of the incident photon energy within the UV-Visible range, which is favorable for efficient charge transfer in DSSC photoanodes [40]. However, at higher photon energies, W-ZnO exhibits increased energy loss, which could impact performance under extreme excitation conditions.

CONCLUSION

ZnO nanoparticles were synthesized via the sol-gel method and characterized using XRD and UV- Vis spectroscopy, showed that annealing enhanced the crystallinity of ZnO, as indicated by sharper and more intense diffraction peaks, along with a steady increase in crystallite size, suggesting grain growth. The computational investigation of the structural, electronic, and optical properties of wurtzite ZnO using DFT, DFT+U_d, and DFT+U_d+U_p approaches demonstrates the progressive improvement in the accuracy of predicted material properties with the inclusion of on-site Coulomb interactions. Structurally, the application of U_d and U_p corrections led to lattice parameters and bond lengths that closely matched experimental values, indicating improved representation of atomic interactions. Electronically, the band gap increased from 0.79 eV (DFT) to 1.45 eV (DFT+U_d) and finally to 3.19 eV (DFT+U_d+U_p) with the latter closely reproducing the experimental band gap, thereby correcting the well-known underestimation in standard DFT. Optically, the incorporation of Ud and Up shifted the dielectric function and absorption edge, improving the alignment with experimental observations. Overall, the DFT+U_d+U_p method proved most reliable in capturing the true behavior of W-ZnO, making it a suitable computational approach for predicting its potential in optoelectronic applications such as dye-sensitized solar cells.

REFERENCES

1. Ahn, M. W., Park, K. S., Kim, D. W., Kim, K. J., Choi, K. J., Lee, G. H., & Park, J. G. (2020). ZnO nanostructures for dye-sensitized solar cells: A review. Journal of Alloys and Compounds, 814, 152208.
2. Wahab, R., Khan, F., Al-Hartomy, O. A., Al-Ghamdi, A. A., & Hwang, J. (2019). Recent developments in ZnO nanostructures for DSSC applications. Ceramics International, 45(14), 17564–17576.
3. Yu, L., Yu, H., Sun, J., & Lin, J. (2020). ZnO nanostructures and their photoelectrochemical properties for solar energy conversion. Journal of Materials Science: Materials in Electronics, 31(2), 1097–1111.
4. Anitha, V. S., Bhattacharyya, D., & Mohan, R. (2020). A review on ZnO nanostructures for photovoltaic applications. Materials Today: Proceedings, 33, 3795–3801.
5. Yao, K., & Wang, X. (2018). Structural and optical properties of ZnO nanorods: DFT and experimental investigations. Optik, 156, 956–962.
6. Agarwal, A., & Nair, M. T. S. (2019). Defect engineering in ZnO for enhanced solar cell applications. Applied Surface Science Advances, 6, 100108.
7. Yin, W.-J., Wei, S.-H., & Al-Jassim, M. M. (2018). DFT + U studies on defect levels in semiconductors. Journal of Physics D: Applied Physics, 51(39), 393001.
8. Perdew, J. P., Burke, K., & Ernzerhof, M. (1996). Generalized Gradient Approximation Made Simple. Physical Review Letters, 77(18), 3865.
9. Shao, Y., et al. (2020). Sol–gel synthesis and DFT study of ZnO thin films for solar energy applications. Journal of Materials Research and Technology, 9(4), 8891–8900.
10. Jiang, J., Li, J., & Sun, Y. (2020). Optical and electronic behavior of ZnO nanostructures for DSSC photoanodes. Materials Science in Semiconductor Processing, 107, 104841.

11. Giannozzi, P., Baroni, S., Bonini, N., Calandra, M., Car, R., Cavazzoni, C., &Wentzcovitch, R. M. (2009). QUANTUM ESPRESSO: a modular and open-source software project for quantum simulations of materials. *Journal of physics: Condensed matter*, *21*(39), 395502.
12. Perdew, J. P., Burke, K., & Ernzerhof, M. (1996). Generalized gradient approximation made simple. *Physical review letters*, *77*(18), 3865.
13. Benrezgua, E., Zoukel, A., Deghfel, B., Boukhari, A., Amari, R., Kheawhom, S., & Mohamad, A. A. (2022). A review on DFT+U scheme for structural, electronic, optical and magnetic properties of copper doped ZnO wurtzite structure. Materials Today Communications, 31, 103306.
14. Achehboune, M., Khenfouch, M., Boukhoubza, I., Derkaoui, I., Leontie, L., Carlescu, A., Mothudi, B., & Zorkani, I. (2022). Optimization of the luminescence and structural properties of Er-doped ZnO nanostructures. Journal of Luminescence, 246, 118843.
15. Shihatha, A. T., Ghelab, A. M., & Munfi, R. A. (2022). Theoretical study of electronic structure and optical properties for ZnO thin film. AIP Advances, 12(2), 020023.
16. Samsonie, A. G., & Morgade, C. I. N. (2021). Morphological, structural, and electronic properties of green synthesized ZnO nanoparticles —A review. Physics Letters Section A, 411, 127712.
17. Karazhanov, S., et al. (2020). DFT+U calculations for electronic, structural, and optical properties of ZnO wurtzite structure: A review. Results in Physics, 16, 102829.
18. Guermit, Y., & Rached, D. R. (2020). Structural and electronic properties of ZnO: A first-principles DFT-LDA/GGA and LDA/GGA+U study. Materials Science and Engineering B, 258, 114590.
19. Rauf, H., et al. (2021). First-principles study of electronic and optical properties of ZnO and its implications for solar cells. Optik, 230, 166375.
20. Kahura, I. M., Kiprotich, S., & Mulwa, W. M. (2024). An ab initio GGA+ U Study of the Wurtzite Structure of ZnO for Dye-Sensitized Solar Cells Application.
21. Alawani, N. A., et al. (2021). Electronic and optical properties of ZnO with different dopants: A GGA+U study. Journal of Alloys and Compounds, 853, 156634.
22. Sharma, R. K., et al. (2020). Optical and structural properties of ZnO nanostructures for DSSC photoanodes. Materials Research Bulletin, 124, 110731.
23. Benrezgua, E., et al. (2022). Effect of Mn doping on structural, morphological, electronic & optical properties of ZnO: Experimental and DFT+U study. Physica B: Condensed Matter, 616, 413766.
24. Bett, K., & Kiprotich, S. (2024). Effects of stirring speed of precursor solution on the structural optical and morphological properties of ZnO Al Ga CoDoped nanoparticles synthesized via a facile sol gel technique.
25. Kahura, I. M., Kiprotich, S., & Mulwa, W. M. (2024). Energy Band-gap Engineering for ZnO as a Photoanode of Dye Sensitized Solar Cells; An ab initio Study.
26. Balamurugan, C., & Sundaram, N. M. (2020). Effect of annealing on the properties of ZnO for solar cell applications. Materials Today: Proceedings, 33, 2345–2349.
27. Zhao, L., & Yu, Y. (2021). Ab initio investigation of optical and electronic properties of ZnO. Computational Condensed Matter, 8, 91-98.
28. Ahn, S., et al. (2021). DFT+U study on ZnO and its intrinsic defects. Journal of Applied Physics, 129(5), 055105.
29. Ungula, J., & Dejene, B. F. (2016). Effect of solvent medium on the structural, morphological and optical properties of ZnO nanoparticles synthesized by the sol–gel method. *Physica B: Condensed Matter*, *480*, 26-30.
30. Ungula, J., Dejene, B. F., & Swart, H. C. (2017). Effect of annealing on the structural, morphological and optical properties of Ga-doped ZnO nanoparticles by reflux precipitation method. *Results in physics*, *7*, 2022-2027.
31. Namisi, M. M., Musembi, R. J., Mulwa, W. M., & Aduda, B. O. (2023). DFT study of cubic, tetragonal and trigonal structures of KGeCl3 perovskites for photovoltaic applications. *Computational Condensed Matter*, *34*, e00772.
32. Naldoni, A., et al. (2021). Band-gap tuning of ZnO by nitrogen doping. The Journal of Physical Chemistry C, 125(3), 7134-7141.
33. Barhoumi, A., et al. (2021). Effect of annealing temperature on ZnO structural and optical properties: Experimental and DFT comparison. Ceramics International, 47(5), 5241-5247.

34. Dzade, N. Y., et al. (2021). Hierarchical ZnO nanowires: combined experimental and DFT study for sensor applications. New Journal of Chemistry, 45(3), 1404-1414.
35. Chen, D., et al. (2021). ZnO/CuSCN nano-heterostructure: experimental and theoretical investigation. ACS Omega, 6(6), 3673-3680.
36. Ghosh, S., Sen, K., Debnath, P., & Mondal, N. (2022). DFT study and photocatalytic activity of ZnO/N-doped TiO_2 heterojunctions. Journal of Physical Chemistry C, 126(12), 5219-5230.
37. Saleem, M., et al. (2021). Solution processed $Zn_{1-x-\gamma}Sm_xCu_\gamma O$ nanorod arrays for DSSCs. Nanomaterials, 11(7), 1710.
38. Malhotra, S. S., Saran, R. K., & Ahmed, M. (2024). DFT studies on metal oxide@graphene systems for DSSC applications. ACS Omega, 9(5), 2561-2572.
39. Kahura, I. M., Kiprotich, S., & Mulwa, W. M. (2024). A DFT Investigation of RE (Ce, Dy, Eu) Doped Monolayer ZnO for Potential Application in Dye Sensitized Solar Cells Application.
40. Kahura, I. M. (2025). Comparative First-Principles Study of Lead-Free $Cs_2AgB'Br_6$ (B′= Bi, Sb, In) Double Perovskites for Photovoltaic Applications.